



# Underwater radiated noise from a submerged cylinder: measurements in far and near field conditions

Matthieu Decaux, Florian Hugues, Quentin Leclère, Laurent Maxit, Valentin Meyer, Cédric Carbonell

## ► To cite this version:

Matthieu Decaux, Florian Hugues, Quentin Leclère, Laurent Maxit, Valentin Meyer, et al.. Underwater radiated noise from a submerged cylinder: measurements in far and near field conditions. Internoise 2023, Aug 2023, Chiba, Japan. hal-04579031

HAL Id: hal-04579031  
<https://hal.science/hal-04579031v1>

Submitted on 17 May 2024

**HAL** is a multi-disciplinary open access archive for the deposit and dissemination of scientific research documents, whether they are published or not. The documents may come from teaching and research institutions in France or abroad, or from public or private research centers.

L'archive ouverte pluridisciplinaire **HAL**, est destinée au dépôt et à la diffusion de documents scientifiques de niveau recherche, publiés ou non, émanant des établissements d'enseignement et de recherche français ou étrangers, des laboratoires publics ou privés.



## Underwater radiated noise from a submerged cylinder: measurements in far and near field conditions

Matthieu Decaux<sup>1</sup>

LVA, INSA Lyon

Laboratoire Vibrations Acoustique, INSA-Lyon, 25 bis avenue Jean Capelle, F-69621 Villeurbanne Cedex, France

Florian Hugues<sup>2</sup>

Naval Group

Naval Group, 199 Avenue Pierre-Gilles de Gennes, 83190, Ollioules, France

Quentin Leclère<sup>3</sup>

LVA, INSA Lyon

Laboratoire Vibrations Acoustique, INSA-Lyon, 25 bis avenue Jean Capelle, F-69621 Villeurbanne Cedex, France

Laurent Maxit<sup>4</sup>

LVA, INSA Lyon

Laboratoire Vibrations Acoustique, INSA-Lyon, 25 bis avenue Jean Capelle, F-69621 Villeurbanne Cedex, France

Valentin Meyer<sup>5</sup>

Naval Group

Naval Group, 199 Avenue Pierre-Gilles de Gennes, 83190, Ollioules, France

Cédric Carbonell<sup>6</sup>

Naval Group

Naval Group, 199 Avenue Pierre-Gilles de Gennes, 83190, Ollioules, France

### ABSTRACT

*Measurements of radiated pressure from a cylinder hull immersed in water are of interest for naval research. Generally, the far-field pressure pattern in a wide frequency range is required. We compare the direct measurement of the far-field underwater noise generated by a vibrating cylinder submerged in a large dock to the far-field prediction obtained via near-field measurements of the same structure in a reverberant tank. Both measurements require advanced signal processing to minimize the impacts of undesired factors such as low signal-to-noise ratio or with disturbing echos. The results associated with both environments are confronted and provide general guidance to evaluate the radiated sound power.*

---

<sup>1</sup>matthieu.decaux@insa-lyon.fr

<sup>2</sup>florian.hugues@naval-group.com

<sup>3</sup>quentin.leclere@insa-lyon.fr

<sup>4</sup>laurent.maxit@insa-lyon.fr

<sup>5</sup>valentin.meyer@naval-group.com

<sup>6</sup>cedric.carbonell@naval-group.com

## 1. INTRODUCTION

Characterization of radiated pressure from a cylinder hull immersed in water is a challenge in many aspects. Measuring far-field radiated sound pressure of submerged structures is usually conducted in large lakes, inner harbors or as sea-trials. These are often expensive and are only used for the final testing of complete systems. Ideally, underwater acoustic experimentation in a test tank can subvert this issue. However, tanks are rarely acoustically treated and it is in practice difficult to achieve a true anechoic environment at low frequencies.

A number of deconfinement methods exist to enable free-field acoustic conditions. One of these techniques called the wave train method [1] consists in measuring the steady-state portion of the received signal with a time-window to isolate the direct-path signal from reflections and transients. Simple geometrical considerations are commonly used to calculate the arrival time of the echoes and therefore the amount of time-domain signal available for the analysis. A limitation is that the acoustic tank size imposes a lower limiting frequency corresponding to a signal portion containing very few time-series data.

Another group of methods makes use of all the received signals including reflections but attempts to eliminate the effect of the reflections using signal processing. The analysis is usually performed in the frequency domain, with signal processing ranging from simple averaging to various forms of deconvolution, windowing or filtering. Examples of such techniques include the cross-correlation method, which uses swept sinusoidal signals and a narrow-band swept filter synchronised to the drive signal. By applying a window on the cross-correlation function it is possible to remove the effect of the boundary echoes if the peaks are narrow enough. Another approach is to use Nearfield Acoustic Holography (NAH). It consists in measuring sound pressure on one surface very near the vibrating surface where reverberated field is supposed to be negligible. However, at low frequencies, the perturbing field has too much energy, and the traditional free field NAH fails to give reliable results [2].

The aim of this paper is twofold. First, we describe several of the practical aspects of far-field and near-field measurement made respectively in a harbor and a water tank. Second, the radiated sound power prediction based on near-field measurements of a submerged cylinder is compared to the direct measurement of the acoustic intensity in the far-field (mean-square pressure) of the same structure.

## 2. MEASUREMENT FACILITIES

Experiments were conducted at two separate places: a harbor and a water tank. Figure 1 shows a schematic of both installations including the locations of the submerged vibrating structure and the hydrophones. Far-field and near-field measurements were applied to a point-driven cylinder with flat circular end caps. The steel cylinder was machined down to obtain a nominal outer diameter of 0.3185 m and wall thickness of 12 mm. The shell has a theoretical in vacuo ring frequency of about 2700 Hz. The critical frequency, found by equating structural bending wave speed to the acoustic wave speed of water is about 19 kHz. The shell has an axial length of 2 m (including the end caps). O-ring seals have been used and were compressed between the end cap seal and the cylinder wall to ensure proper sealing. Due to the large amount of air in the submerged cylinder, extra weights were added to ensure neutral buoyancy. The cylinder's external surface was treated with an epoxy painting process for anti-corrosion purposes which gives its white appearance. The structure was excited using a small inertial shaker mounted in the inner face of the shell wall. A force transducer was rigidly fixed between the shaker stinger and a threaded hole to measure the force exerted on the shell. The generation was controlled via a custom-made, underwater cable (MacArtney) that contained coaxial connections. In both environments, data were acquired for a frequency range of 200 Hz to 5 kHz. Band limited Gaussian white noise and swept frequency-modulate pulse were used to drive the shaker. Simultaneous averaged frequency response functions were recorded between the shaker force input and the hydrophones. The hydrophones used to measure sound pressure were

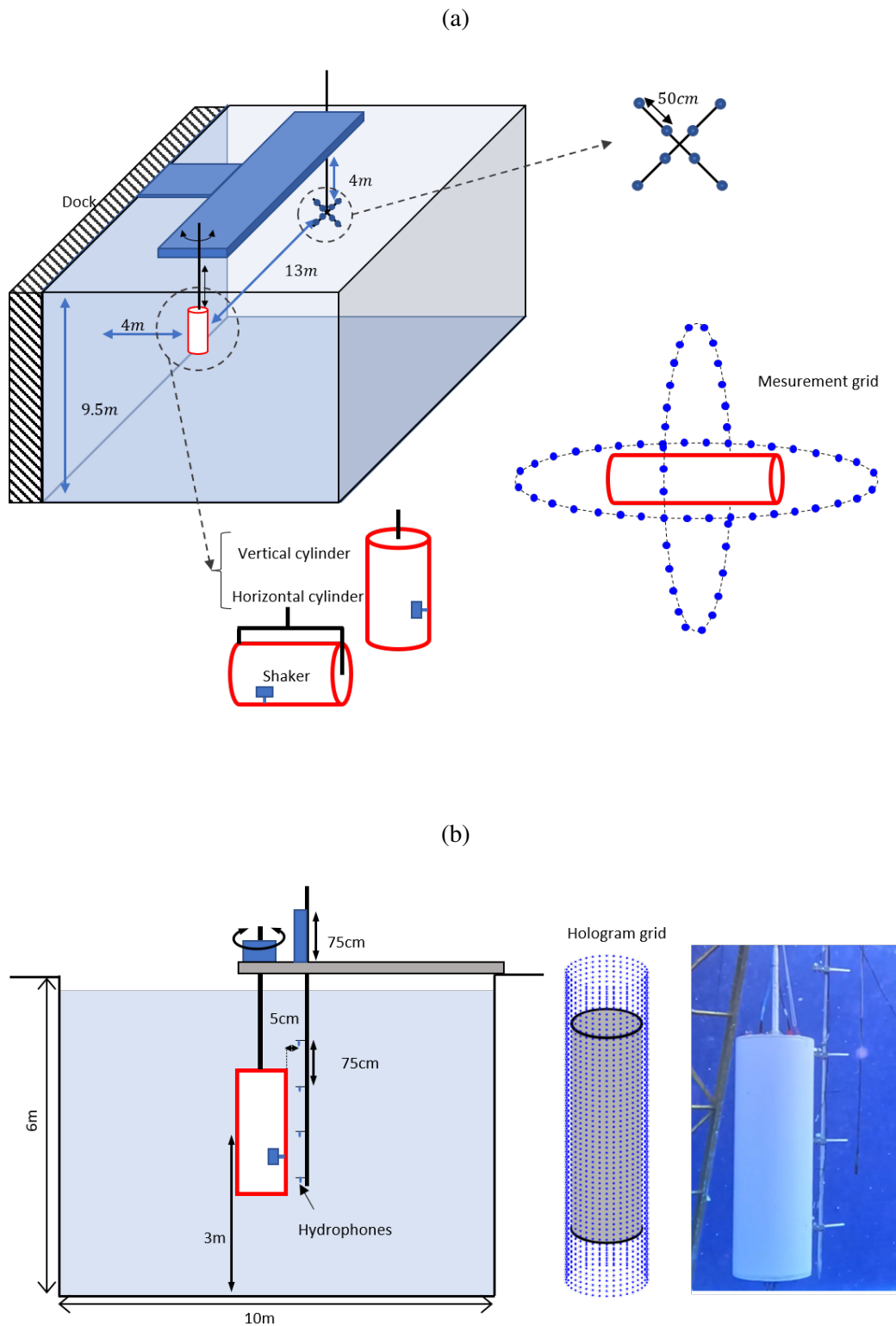


Figure 1: Scheme of the 2 setups used for the measurements, (a) dock experiment for far-field measurements; (b) tank experiment for near-field measurement.

Neptune model B/200 miniature. These hydrophones have a nominal receive sensitivity of  $-212.5$  dB ref  $1\text{ V }\mu\text{Pa}^{-1}$ . They were connected to a B&K Type NEXUS charge amplifiers for conditioning of the signal before it was applied to a B&K LAN-XI data acquisition hardware.

The parameters used to compute spectra are the same for both configurations. The sampling frequency used is  $65\,536$  Hz. A frequency resolution of  $1$  Hz is chosen with a Hanning window and  $66\%$  overlap. The global coherence function is introduced to assess the global uncertainty of the measured frequency response functions between the force input and the hydrophones. This indicator is obtained in the manner of Roozen *et al.* [3] as

$$\Gamma_{global} = \frac{\langle \Gamma_{pf} S_{pp} \rangle_N}{\langle S_{pp} \rangle_N}, \quad (1)$$

where  $\Gamma_{pf}$  is the usual coherence function of a single-input single-output system, *i.e.*  $\Gamma_{pf} = \frac{|S_{pf}|^2}{S_{pp} S_{ff}}$ ,  $S_{pp}$  is the auto-spectrum of the pressure,  $S_{ff}$  is the auto-spectrum of the injected force,  $S_{pf}$  is the cross-spectrum of the pressure and injected force and  $\langle \dots \rangle_N$  denotes the arithmetic mean over all  $N$  measurement points. This formula can be seen as the ratio of the mean coherent auto-spectrum by the mean of the total auto-spectrum.

## 2.1. Dock measurements

A diagram of the dock measurement setup is given in Figure 1a. The underwater acoustics facility consists in a rectangular raft that has an opening in the front through which the cylinder is hung with a hoisting mast system. It is  $4$  m away from the dock, and the sea level is about  $9.5$  m. The cylinder acoustic center has been lowered to  $4$  m below the water surface. The hoisting motor allows a  $360^\circ$  rotation of the cylinder and it is operated via a control panel. Two different flanges have been designed to lift and rotate the vibrating cylinder vertically and horizontally. These two configurations enable directivity measurements in both elevation and azimuth. The rectangular raft has an opening in the middle through which hydrophones can be immersed at different points from the cylinder. In front of the vibrating cylinder, an X-shaped hydrophone array is hung vertically at approximately mid-width and mid-depth. It is composed of  $8$  hydrophones (separated by  $50$  cm, spanning  $1.5$  m) and the X shape has been chosen so that the effect of reflections from above (platform) and from the side (dock) can be reduced. The theoretical radiation pattern of this array shows that the echos from above (raft) and from the side (dock) can be attenuated by at least  $3$  dB from  $500$  Hz to  $2000$  Hz. The receiving array is located  $13$  m from the cylinder. The directivity pattern measurements were carried out by rotating the cylinder by steps of  $10^\circ$  for the two positions. This gives  $2 \times 35$  unique points where the far field pressure is measured.

Figure 2a shows the averaged SNR measurements recorded at all hydrophone positions in the dock. The background noise is depicted in black for three different varying background noise levels over the course of the trials. This noise level is compared to the levels of the sea's ambient noise according to the Knudsen scale [4]. It shows a significant variation throughout the day (sea state from  $3$  to  $6$ ) depending on industrial activity in the harbor area. The pressure signal radiated by the vibrating cylinder is reported in blue. For nominal conditions, the SNR increases with frequency about  $5$  dB below  $1000$  Hz and stays above  $30$  dB up to  $3000$  Hz. It decreases slightly to  $15$  dB at  $5000$  Hz. The global coherence indicator is given Figure 2b. This result shows statistically significant coherence detected in most signal-pairs at frequencies corresponding to the resonant frequencies of the cylinder. For frequencies greater than  $1000$  Hz, the global coherence indicator has a median value reaching  $0.95$ , indicating an acceptable correlation. A drop at about  $4000$  Hz can be observed due to the drop in SNR.

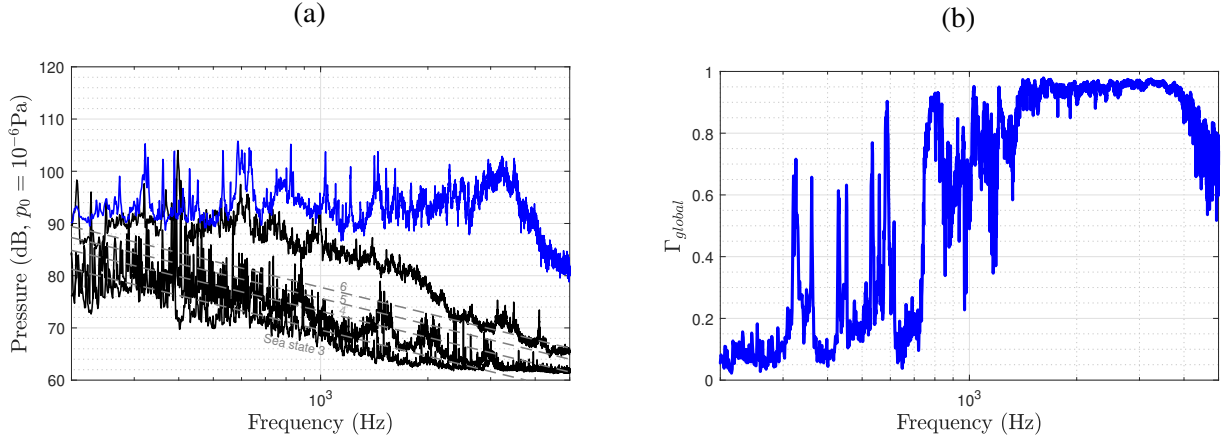


Figure 2: (a) Level of the radiated pressure from the cylinder in the dock environment (—) with 3 samples of background noise (—). (b) Global coherence function between the injected force and the measured pressure.

## 2.2. Water tank measurements

The outdoor test tank located at Ifremer, La Seyne sur Mer, has an area of  $15 \times 10 \text{ m}^2$  and a depth of 6 m. Unlike the previous environment, the water tank involves rigid side walls. A schematic presentation of the facility is shown in Figure 1b. The water tank was specially instrumented with a computer-controlled positioning system to perform NAH measurements. The same cylinder used in the harbor was submerged in the water tank and suspended from a rotating arm that is screwed into the rotary stage of the positioning system. A boom with a set of 4 hydrophones equally spaced was attached directly to an elevation stepper motor. The NAH scanning procedure was carried out under computer control by moving vertically the boom in successive steps and recording the time pressure at each position. After a complete vertical scan (61 positions are measured for a total aperture of 3 m), the cylinder was rotated by  $10^\circ$ , and the axial scan was repeated. A cylindrical hologram was obtained resulting in 2196 total measurement points. This was repeated only 2 times for each position due to the limited duration of the test campaign. The radial distance between the hologram and the cylinder surface (also called the standoff distance) was set at about 5 cm. Ballast weight hung from the center of the cylinder bottom end cap was added to prevent positioning errors and keep constant the radius of the cylindrical hologram. The rotating arm was designed to be rigid enough and could be adjusted so that the cylinder hangs and rotates with minimum precession resulting in a positioning error of less than 1 cm. The positioning system was computer-controlled via a custom user interface in NI LabVIEW. Note that the following procedure is lifted mostly from the thorough development of Barnard [5] and the reader is referred to the standard textbook of Williams [6] for further details on the NAH implementation.

Figure 3a shows the averaged SNR measurements recorded at all hydrophone positions in the tank. The background noise is drawn in black. Being next to a large building the electromagnetic perturbation is present at 50 Hz and all of its harmonics. The pressure signal radiated by the vibrating cylinder is reported in red. For nominal conditions, the SNR is above 60 dB for the considered frequency range. The global coherence indicator is given Figure 3b. Except for the 50 Hz harmonics, and above 300 Hz, the global coherence indicator is above 0.9, indicating an acceptable correlation. Electromagnetic noise is reduced using coherent signal processing from Bendat and Piersol [7].

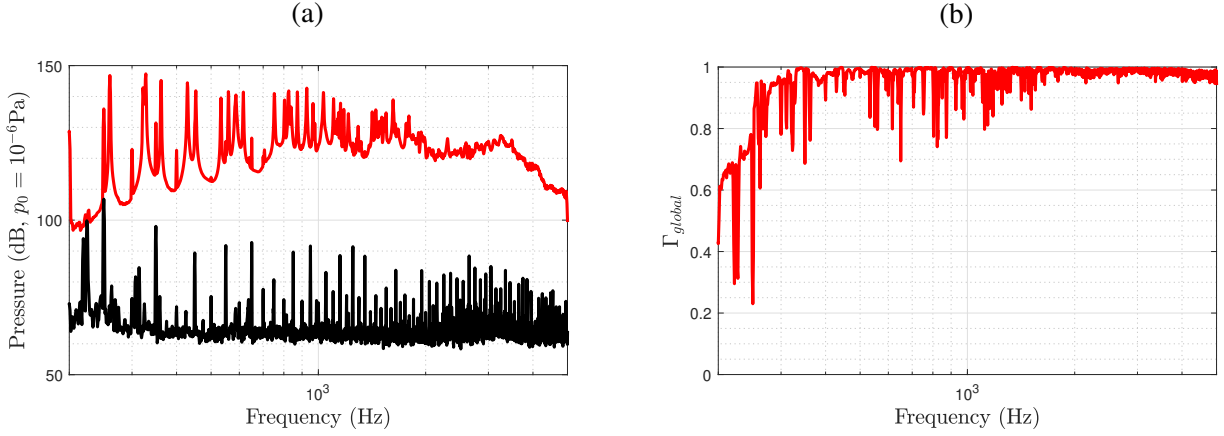


Figure 3: (a) Level of the radiated pressure from the cylinder into the water tank (—) compared to the background noise (—), (b) Global coherence function between the injected force and the measured pressure.

### 3. DATA PROCESSING THEORY

#### 3.1. Echo removing using the cross-correlation technique

The cross-correlation technique has been considered in an attempt to eliminate the effect of echoes, the mathematical background is briefly introduced. The cross-correlation between two signals  $x$  and  $y$  is defined as

$$R_{xy}(\tau) = \int_{-\infty}^{\infty} x(t)y(t - \tau)dt, \quad (2)$$

where  $\tau$  is a time delay. In the case of echos, the measured signal can be expressed as the sum of signals delayed by  $d/c$ , where  $d$  is the propagation distance and  $c$  the sound speed in water. The new cross-correlation can be expressed as

$$R_{xy}(\tau) = R_{xy_0}(\tau - d_0/c) + \sum_{i=1}^{\infty} R_{xy_i}(\tau - d_i/c), \quad (3)$$

where  $R_{xy_0}$  is the cross-correlation of the direct field, and  $R_{xy_i}$  is the cross-correlation of the echos. If the contributions are short enough, a window can be applied to select only the direct field. The cross-spectral density  $\hat{G}_{xy}$  can be calculated according to

$$\hat{G}_{xy} = \mathcal{F}\{\hat{R}_{xy}(\tau)\}, \quad (4)$$

where  $\hat{R}_{xy}(\tau)$  denotes the windowed signal and  $\mathcal{F}$  the Fourier transform operator.

#### 3.2. Direct measurement of the far-field radiated pressure

The radiated power is defined by the integration of the acoustic intensity over a control surface  $S$  enclosing the source

$$\Pi = \int_S I_r dS. \quad (5)$$

In the far field, the acoustic intensity can be expressed as  $I_r \approx \frac{|P|^2}{2\rho c}$ , where  $\rho$  is the density of water and  $P$  the complex amplitude of the acoustic pressure at a given frequency. An approximation of the radiated power can be expressed as

$$\Pi \approx \frac{S}{2\rho c} \frac{1}{N} \sum_{j=1}^N |P_j|^2, \quad (6)$$

where  $P_j$  is the pressure at the  $j^{\text{th}}$  point of the measurement grid. This far-field pressure is evaluated as the mean of the pressure measured by the eight hydrophones for each measurement point. Note that the summation over all the hydrophones can be assimilated as a beamforming steering in the direction of the cylinder. In our case, the time delay is less than a sampling period, and therefore it is neglected. By applying this technique, it is found that the level is reduced by 3 dB between the resonances.

### 3.3. Prediction of radiated pressure based on Nearfield Acoustic Holography

Nearfield Acoustical Holography (NAH) is a well-known technique mainly used for the identification and localization of noise sources. The spectral pressure coefficients  $P_n(r_h, k_z, \omega)$  are found by taking the two-dimensional Fourier transform of the acoustic pressure  $p(r, z, \theta, \omega)$  measured on the hologram. Note that these quantities are complex, possessing both amplitude and phase (relative to the input force signal) information. By using the so-called stationary phase theorem, the far field radiated pressure can be determined from

$$p_\infty(r, \theta, \phi, \omega) = \frac{e^{jkr}}{\pi r} \sum_{n=-N}^N (-j)^{n+1} e^{jn\theta} \frac{P_n(r_h, k \cos \phi)}{H_n^1(kr_h \sin \phi)}, \quad (7)$$

where  $k_r = \sqrt{k^2 - k_z^2}$  is the radial wave-number,  $k = \omega/c$  is the acoustic wave-number,  $H_n^1$  is the Hankel function of the first kind,  $N \approx ka \sin \phi$ , and  $(r, \theta, \phi)$  are the spherical coordinates of the measured pressure. The spherical coordinates convention used in this formula is given in Figure 4. The expression of the radiated power  $\Pi$  is given by

$$\Pi(\omega) = \frac{1}{\pi \rho c k} \int_{-k}^k \sum_{n=-\infty}^{\infty} \left| \frac{P_n(r_h, k_z)}{H_n^1(k_r r_h)} \right|^2 dk_z. \quad (8)$$

The truncation in the axial direction reveals no power is radiated by subsonic waves ( $|k_z| > k$ ). In the circumferential direction, no truncation is explicitly introduced but the power drops off rapidly above  $n = ka$ . Note that in the given theory, the temporal convention is  $e^{-j\omega t}$ .

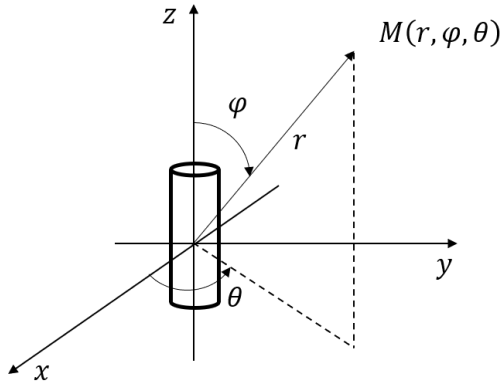


Figure 4: Convention for spherical coordinates in the NAH method.

## 4. RESULTS

### 4.1. Crosscorrelation technique to remove echoes

The cross-correlation technique is employed to highlight the effect of the reverberation. Figures 5a and 5b show the normalized cross-correlation for respectively a calibration source and the cylinder in both configurations. The normalization enables comparison of the different setups by scaling the

results between -1 and 1. Using a calibration source, the direct field and the first reflection can be identified and windowed. In both configurations, the source was about 2 m from the hydrophone. After 10 ms the cross-correlation is near zero for the far-field configuration while the reflections for the tank are visible. The cross-correlation technique requires enough time between the direct field and the first echo. This is illustrated using the cylinder. The structure transient response narrows the bandwidth of the transmitted acoustic signal, which means that the peaks in the cross-correlation signal are broadened making it difficult to distinguish the peaks and therefore window out the reflections.

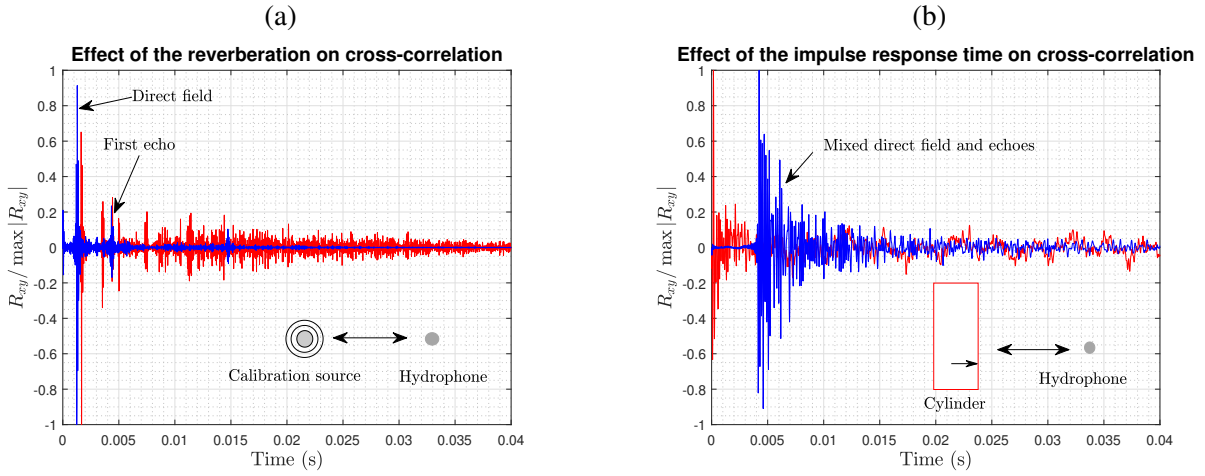


Figure 5: Normalized cross-correlation between the input voltage driving the source and the measured pressure for a sweep in the tank (red) and in the harbor (blue) (a) using a calibration source, (b) using the cylinder.

#### 4.2. Validation of the holography procedure

Figure 6 shows the spectral pressure summed over the circumferential orders. Three areas can be separated by the acoustic wavenumber  $k$  and the flexural wavenumber  $k_f$ . The low-wavenumber components inside the acoustic domain are supersonic (propagating); high wavenumber components are subsonic, or evanescent, and do not radiate sound pressure in the far-field. Components higher than the flexural wavenumber are filtered by the structure, the elastic nature of the cylinder limits the spectrum from exhibiting extremely small variations in space (high wavenumber). In the low frequency, the energy is spread across the subsonic and supersonic domains. Above 4 kHz it appears that the acoustic filtering effect is significant as the energy is concentrated in the acoustic domain. This emphasizes the need of filtering the subsonic wavenumbers in low frequency.

Figure 7 shows the estimated radiated sound power from near-field measurements using two different techniques. On one hand, the power is calculated by the NAH theory Equation 8. On the other hand, the power is estimated by propagating the pressure using the stationary phase theorem Equation 7 to the far-field measurement grid. Even though the grid is sparse and cannot represent accurately the directivity the two methods show a good agreement with less than 3 dB difference, except for two resonances with 5 dB difference. The peaks level are reported table 1. This validates the use of the far-field measurement grid to estimate the radiated power.

#### 4.3. Estimation of the radiated power

Figure 8 shows the direct measurement of the acoustic intensity in the far-field (mean-square pressure) and the NAH. Between the resonances, the measurement made in the far field can be 10 dB above the NAH, in particular in the low-frequency range. This difference should be improved by having longer

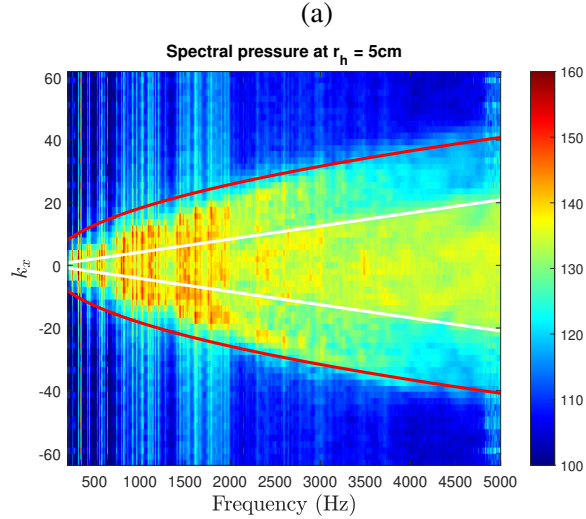


Figure 6: Spectral pressure measured in near field (in dB) summed over the circumferential modes for the hologram at 5 cm. The acoustic cone ( $k = \omega/c$ ) is plotted in white and the bending wave number of the equivalent plate is in red.

Frequency (Hz)	322	328	362	429	452	533	560
<b>NAH (dB)</b>	73	75	67	67	63	69	64
<b>Stationary phase (dB)</b>	73	72	66	69	61	70	59
<b>Difference (dB)</b>	+0	-3	-1	+2	-2	+1	-5
Frequency (Hz)	586	616	804	826	873	927	1033
<b>NAH (dB)</b>	67	62	68	75	68	66	72
<b>Stationary phase (dB)</b>	69	63	68	70	66	65	72
<b>Difference (dB)</b>	+2	+1	+0	-5	-2	-1	+0

Table 1: The first 14 peaks identified in figure 8 plotting the sound power estimation using different methods: NAH power and propagation of the hologram using stationary phase

recordings, and thus more averages reducing incoherent background noise contribution. Nonetheless, most of the peaks are measured within  $\pm 3$  dB difference. For an easier comparison, their level and difference relative to the NAH power are reported in Table 2. It can be noted that two frequencies are emerging at 389 Hz and 410 Hz in the far field measurement. This is probably linked to the industrial activity nearby as these frequencies can be identified in some background noise measurements. Three resonances, 328 Hz, 586 Hz and 1033 Hz, vary by respectively  $-8$  dB, 7 dB and 5 dB. Above 1 kHz, both measurements agree well, and the difference is acceptable for the purpose of this study.

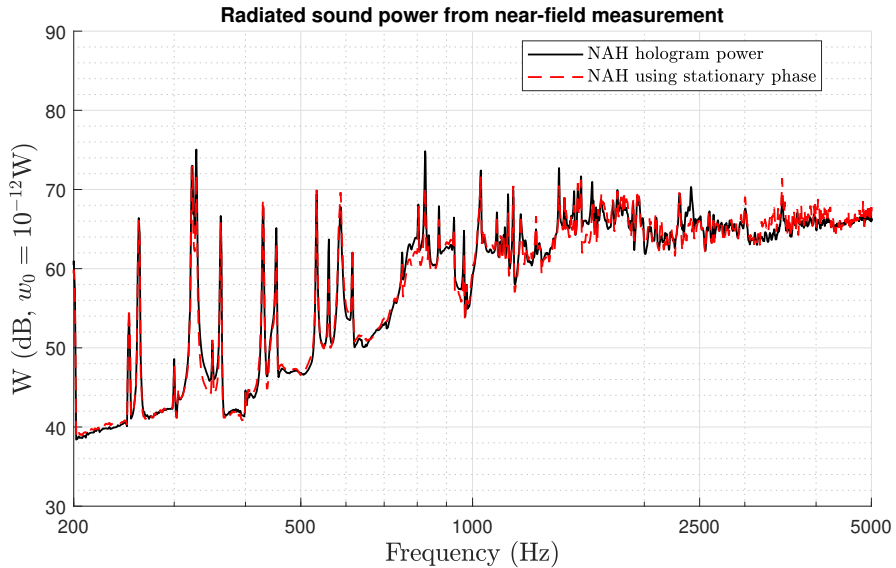


Figure 7: Radiated power from the near-field measurement, estimated by the stationary phase propagated to the far-field measurement grid or using the NAH theory

Frequency (Hz)	322	328	362	429	452	533	560
<b>NAH (dB)</b>	73	75	67	67	63	69	64
<b>Direct measurement (dB)</b>	71	67	67	69	66	72	64
<b>Difference (dB)</b>	-2	-8	+0	+2	+3	+3	+0
Frequency (Hz)	586	616	804	826	873	927	1033
<b>NAH (dB)</b>	67	62	68	75	68	66	72
<b>Direct measurement (dB)</b>	74	59	66	76	67	65	77
<b>Direct measurement (dB)</b>	+7	-3	-2	+1	-1	-1	+5

Table 2: The first 14 peaks identified in figure 8 plotting the sound power estimation from the far-field and the near-field measurements

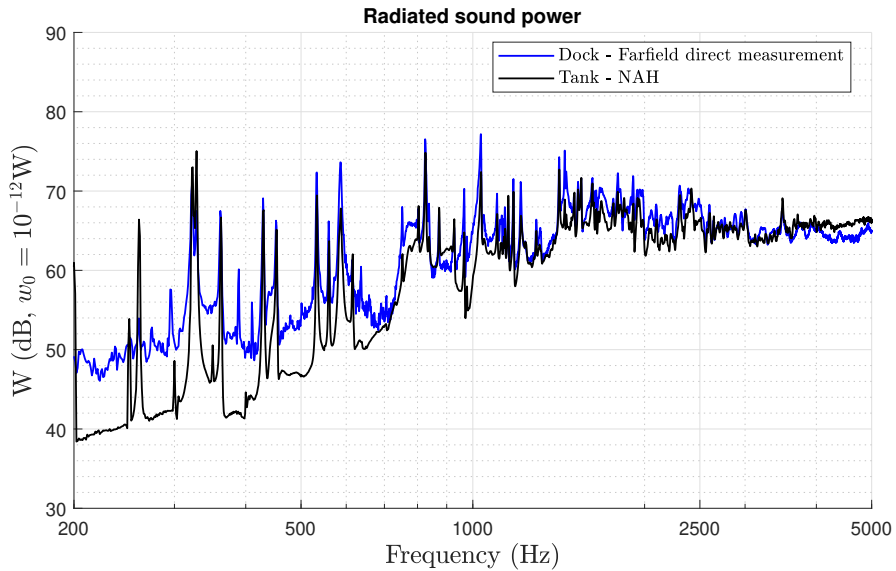


Figure 8: Radiated power of the cylinder estimated from the direct far-field measurement and predicted by the NAH theory.

## 5. CONCLUSIONS

The comparison of the radiated power by a cylinder measured in near-field or far-field has been proposed. The paper tries to point out the practical aspects of the two measurements. On one hand, the SNR is very good in a tank but it is an indirect method and the reflection might pollute the measure. On the other hand, the SNR for the measurements in the far field can be very low (especially in the low frequencies) but the measured pressure is directly accessible since the method is very straightforward.

The estimated radiated sound power for both configurations shows good agreement on the resonances in the low frequency and for the overall level above 2 kHz. By studying the spectral pressure deduced from the hologram, it has been observed that the only significant components are in the acoustic domain for these frequencies. Although the distance from the shell is small, the acoustic filtering effect is significant above 4 kHz.

In the next future, the NAH technique based on the simultaneous use of the two holograms (to deduce the acoustic velocity) should be investigated as well as the ability of this technique to predict the radiation directivity.

## REFERENCES

1. S. P. Robinson. Review of methods for low frequency transducer calibration in reverberant tanks. 1999.
2. A. R. Barnard, S. A. Hambric, and J. D. Maynard. Underwater measurement of narrowband sound power and directivity using supersonic intensity in reverberant environments. *Journal of sound and vibration*, 331(17):3931–3944, 2012.
3. N. B. Roozen, Q. Leclere, M. Rychtarikova, and C. Glorieux. A global error estimator for the uncertainty of a multi-channel spectral analysis. *Applied Acoustics*, 87:57–63, 2015.
4. V. O. Knudsen, R. S. Alford, and J. W. Emling. Underwater ambient noise. *J. Mar. Res.*, 7(3):410–429, 1948.
5. A. R. Barnard. *Development of Supersonic Intensity in Reverberant Environments (SIRE) with applications in underwater acoustics*. PhD thesis, 2010.
6. E. G. Williams and J. A. Mann III. Fourier acoustics: sound radiation and nearfield acoustical holography, 2000.
7. J. S. Bendat and A. G. Piersol. *Random data: analysis and measurement procedures*. John Wiley & Sons, 2011.